JOURNAL OF MATERIALS SCIENCE, 30 (1995) 5543–5550

Characteristics of porosity in solder pastes during infrared reflow soldering

Y. C. CHAN, D. J. XIE*, J. K. L. LAI‡
Department of Electronic Engineering, and ‡ Department of Physics and Materials Science, City University of Hong Kong, Tat Chee Avenue, Kowloon, Hong Kong

The effects of solder pastes and infrared reflow temperature profiles on the characteristics of porosity in solder joints are described. Porosity in solder joints can be detected by X-ray radiography. It was found that the composition and structure of solder pastes had the most significant effect on pore formation. However, a lower metal content and/or a higher heating rate did not necessarily cause a higher percentage of pores in solder joints. Results of experiments on pore formation processes during the whole infrared reflow soldering cycle show that high area fraction of pores in solder joints correspond to the peak temperatures in infrared reflow temperature profiles. To evaluate the thermal effect on the performance and structure of solder pastes, tests were also conducted using differential scanning calorimetry, thermogravimetric analysis (TGA) and weight loss in infrared reflow. It was found that the weight loss rate in the TGA curve and infrared reflow and floating speed of porosity are useful to predict the pore formation behaviour in the solder joint. It is recommended that an IR reflow process is chosen to fit with a suitable solder paste in order to decrease porosity in surface-mount solder joints.

Nomenclature

A	Area sum of pores
A_i	Area of one pore
C	Constants
d, d_i	Diameter of a pore
$d_{i,max}$	Maximum axial dimension of a pore
$d_{i,min}$	Minimum axial dimension of a pore
g	Gravitation constant
L_j	Length of a copper land
M	Atomic weight of alloy
M_1, M_2	Atomic weight of pure metals
n	Number of molecules of gas
P_a	Atmospheric pressure
P_g	Internal gas pressure in a gas bubble
P_h	Hydrostatic pressure
P_s	Shrinkage pressure
R	Gas constant
r	Radius of a pore
S_j	Area of a copper land
S	Area sum of copper lands
T, T_i	Temperature
T_m	Melting point of alloy
V	Volume of a pore
V_m	Atomic volume at the melting point
W_j	Width of a copper land
w, w_i	Weight loss of solder paste
x_1, x_2	Mole fraction in alloy
ε	Area fraction of pores
ε_V	Volume fraction of pores
β	Slope of TGA curve
ρ	Density of liquid alloy
ρ_m	Density of liquid alloy at the melting point
ρ_p	Tap density of solder paste
ρ_s	True density of solder metal
η	Viscosity of liquid solder metal
ν	Rising speed of a gas bubble
γ	Surface tension at the gas–metal interface

1. Introduction

Solder pastes as joining materials are widely used in electronics assembly as surface-mount components become more and more popular. When using solder pastes, however, one major type of defect found in solder joints is porosity. Porosity in surface-mount joints will potentially cause weakening in joint strength and reduction in electrical and thermal conductivity. Furthermore, it will induce crack initiation and shorten the fatigue life of solder joints [1, 2].

A solder paste normally contains 35–65 vol. % volatile materials (e.g. flux and vehicle) [3]. Many flux fumes will be produced during reflow soldering due to thermal decomposition. Some gases may be entrapped between the flat surfaces of the printed circuit board (PCB) and component lead, and cause pore formation in solder joints upon cooling. Therefore, pore

* *Permanent address*: Department of Materials Science, Huazhong University of Science and Technology, Wuhan, People's Republic of China.

0022–2461

formation is related to the solidification characteristics of the solder.

The pore formation process begins with nucleation of a gas bubble. In order to sustain a macroscopic bubble in a freezing melt, the following pressure equilibrium should be obtained [4]

$$P_g + P_S = P_h + P_a + 2\gamma/r \quad (1)$$

where $2\gamma/r$ represents the pressure produced due to surface tension in a bubble.

There is a critical size of the bubble, r^*, below which the bubble is not capable of surviving and above which the bubble will tend to grow [5]. Because there are many gaseous materials in solder paste, the bubble is simply nucleated in the solder joint. Once a gas bubble is nucleated, it will grow and move only when the internal pressure ($P_g + P_s$) exceeds the external pressure, i.e.

$$P_g + P_S \geqslant P_h + P_a + 2\gamma/r \quad (2)$$

The hydrostatic pressure, P_h, and atmosphere pressure, P_a, can prohibit the gas bubble from growing. Therefore, there are two ways to control the porosity in a freezing metal:

(i) prohibiting the growth of a gas bubble: to reduce the gas formation by reducing the heating temperature and increase the external pressure by using pressurized air. Practically, it is difficult to use these methods;

(ii) promoting growth of the gas bubble: to increase the gas pressure by increasing the temperature, or to decrease the external pressure by using vacuum soldering technology that has been recommended by some researchers [6].

Pore nucleation is also influenced by impurities and interfaces such as inclusions, gas bubble surfaces, and dendritic solidification interfaces. Inclusions such as oxide and rosin can act as effective nuclei for gas holes. Pores easily form at interfaces because little interfacial energy is needed there.

Normally, there are three types of pore-growth behaviour:

(i) small bubbles may accumulate to become a large one which floats away from the interface and escapes from the liquid at the free surfaces;

(ii) small bubbles become entrapped if they are rapidly overgrown by the interface;

(iii) small bubbles grow with the movement of the interface and become entrapped in due course.

For surface-mount soldering, the first two types of pore growth are just what we need. Further, it is hoped that pores will appear early enough and can disappear completely so that no trace of them can be found.

The time available for the growth and escape of a gas bubble will depend on the solidification time of the metal and cooling rate. A bubble may be entrapped if the solidification of the melting is fast enough, and a small-size pore will remain in the metal.

The melting and solidification characteristics of a metal are also influenced by the heating process. Many temperature profiles in infrared reflow soldering can be used. Usually, there are two types of temperature profile for eutectic solder paste [1] :

(a) long and slow preheating to ensure sufficient evaporation of volatile materials in solder pastes;

(b) high preheating and ramp-up speed to obtain a better solder joint [7].

It is often considered that the temperature profile in (b) will result in pore formation in solder joints more readily than that in (a). However, it is worth studying because the processes of gas evaporation and solder solidification are complicated.

X-ray radiography has been successfully used to detect pores in welding joints, castings and other metals [8]. It is now widely used in the mass production of electronics assembly because it is non-destructive and convenient. While a X-ray photograph can only represent a uni-directional view of the solder joint, it is difficult to determine the volume fraction of pores. However, we can determine it quantitatively from X-ray photographs and obtain an area fraction of pores from the following equation

$$\varepsilon_v = A/S \quad (3)$$

The aim of this study was to investigate the effects of solder pastes and infrared reflow processes on pore formation and to obtain a comprehensive model of pore formation mechanisms in surface-mount solder joints.

2. Experimental procedure

2.1. Experimental procedure

Several solder pastes used in the experiments are shown in Table I. All the pastes belong to the mildly activated rosin (RMA) and no-clean type, except Paste 3, which is activated rosin (RA) type.

The specimen selected for the experiments was an FR-4 PCB plate with different copper pad areas on it, as shown in Fig. 1. The land area varies from 0.4×2.50 to 2.5×2.5 mm^2. Solder pastes were deposited to the pre-cleaned copper lands by means of a pneumatic dispenser. The thickness of the solder paste was about 0.25–0.35 mm, which was obtained from laser section microscopy (LSM, CyberOptics Corporation). In order to minimize the variables in the characteristics of pore formation, no components or other objects were placed on the copper land except solder pastes. The specimen was also termed a blank land sample or

TABLE I Solder pastes chosen in the experiments (Multicore Solders Ltd and Alpha Metals Hong Kong Ltd)

Paste	Alloy	Metal content (wt%)	Flux type	Viscosity (10^6 cP)	Average size (μm)
1	Sn63/Pb37	90	RMA	0.8–1	64.0
2	Sn62/Pb38	90	RMA	0.8–1	39.0
3	Sn63/Pb37	90	RA	0.8–1	39.0
4	Sn63/Pb37	90	RMA	0.8–1	44.0
5	Sn63/Pb37	88	RMA	0.66	60.0
6	Sn63/Pb37	86	RMA	0.4	39.0

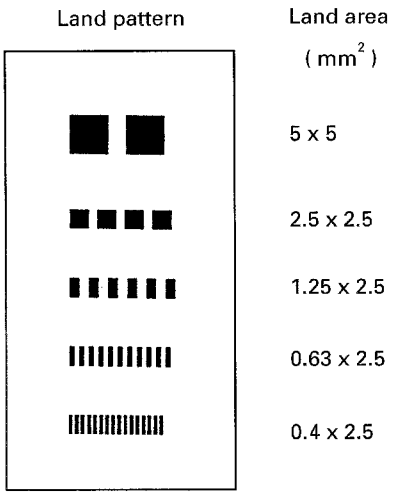

Figure 1 PCB copper land pattern.

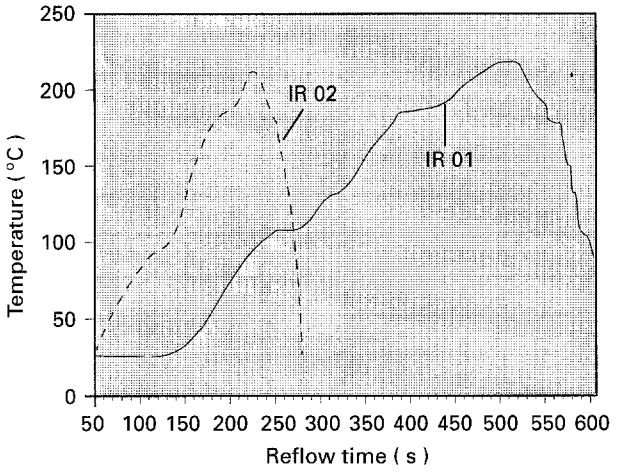

Figure 2 The two types of infrared reflow temperature profile used in the experiments.

blank solder joint. The specimen was then reflowed in the infrared reflow machine (type Heller 932). Two types of reflow temperature profile, IR 01 and IR 02, were determined, as shown in Fig. 2.

2.2. Calculation of area fraction of pores

During X-ray observation, the PCB plate was placed perpendicular to the X-ray beam so that the largest cross-section of the solder joints could be seen. In a practical assembly, fatigue failure normally originates from that cross-section of the solder joints.

Normally, gas pores found in X-ray photographs are circular or near circular in shape. Thus, we can calculate the area of a pore by using the average diameter

$$d_i = (d_{i,max} + d_{i,min})/2 \quad (4)$$

$$A_i = \pi d_i^2/4 \quad (5)$$

Each pad area is

$$S_j = W_j L_j \quad (6)$$

Then, the area fraction of porosity in a sample is

$$\varepsilon = \Sigma A_i/\Sigma S_j \quad (7)$$

For a sample which has not been reflowed, X-ray radiography is not applicable to detect pores, because the unreflowed solder paste is in a powder state and has many interfaces. In that case, the solder joint can be considered as a tapped powder. Then the volume fraction of pores, ε_v, can be calculated from the following equation [9]

$$\varepsilon_v = 1 - \rho_p/\rho_s \quad (8)$$

For solder paste Sn63/Pb37, $\rho_p \cong 4.6\ g\,cm^{-3}$ and $\rho_s = 8.3\ g\,cm^{-3}$ [1], then we obtain $\varepsilon_v \cong 44.6\%$. Thus a volume fraction of pores of 44.6% exists in the wet solder paste.

3. Results and discussion

3.1. Pores in different areas of copper pads

Fig. 3 shows pore formation in copper lands with different areas. The solder pastes chosen were Pastes 1 and 3, and the infrared reflow profile was IR01. It is clear from these figures that different land areas have little effect on the dimensions and numbers of pores. For all the five patterns selected, Paste 1 has 3–4.5 area percentage of pores, while Paste 3 has as little as 0–0.4 area percentage of pores. Therefore, the composition and structure of solder pastes have the largest effects on pore formation. We chose a land area of $1.25 \times 2.5\ mm^2$ blank pad sample unless otherwise stated in the following experiments.

3.2. Effect of solder pastes on the pore formation

Solder pastes are homogeneous blends of pre-alloyed solder powder and flux media. The combinations of flux, flux content, viscosity, particle size and shape will affect porosity in joints significantly. Fig. 4 shows the results of pore formation when different kinds of solder pastes are soldered under two reflow temperature profiles. It can be seen that Paste 1 has the highest percentage of pores, followed by Pastes 4 and 5. In Pastes 2 and 3, very few pores are found. In Paste 3,

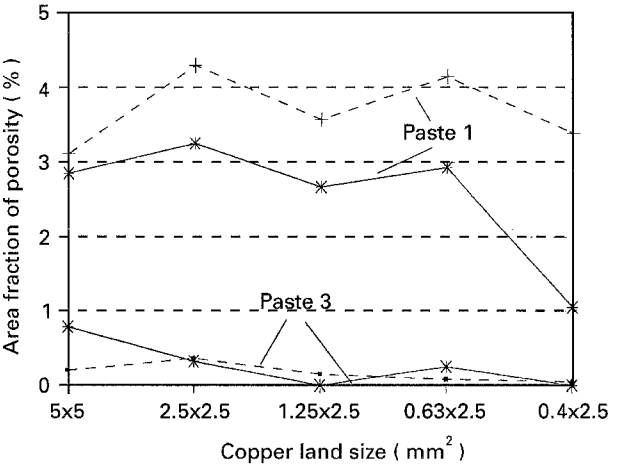

Figure 3 Effects of different copper land areas on pore formation. (+) IR 01, P1; (*) IR 02, P1; (■) IR 01, P3, (*) IR 02, P3.

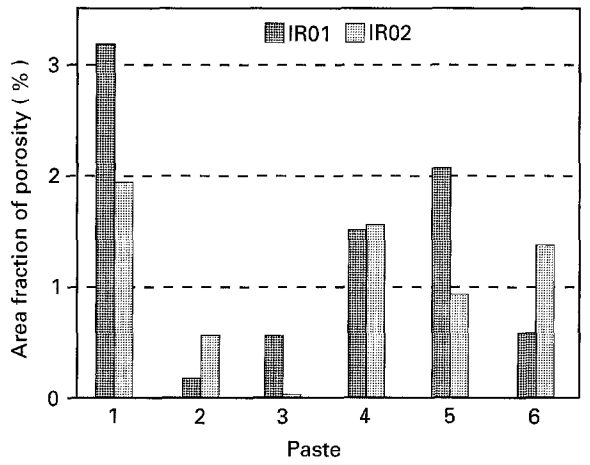

Figure 4 Pore formation of different solder pastes under two infrared reflow files.

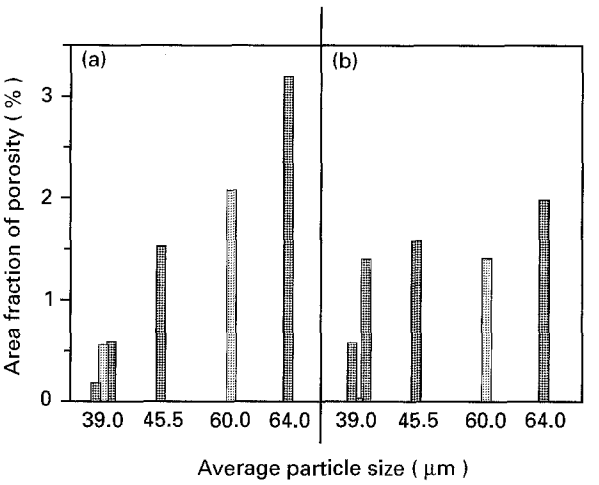

Figure 5 Dependence of area fraction of porosity on the average particle size of a solder paste. Infrared reflow file: (a) IR 01, (b) IR 02.

almost no pores appear if reflowed under temperature profile IR 02. For the majority of these pastes, pore formation behaviour under these two IR reflow temperature profiles is quite different. To decrease pore density, a slower heating rate is more suitable for Pastes 2, 4 and 6, while a faster one is appropriate for Pastes 1, 3 and 5.

Upon rearranging the data according to average particle size of metal powder, we obtain two figures. Interesting enough, as shown in Fig. 5, pore formation has a positive correlation with average particle size in both infrared reflow temperature profiles. The reason may be that the larger particle powder material has a greater percentage of porosity before melting and needs a longer melting time. These pores cannot be eliminated entirely while melting and will remain in the joints after solidification, if heating and cooling periods are not sufficiently long, as we can see in profile IR 02. However, further investigation is needed to confirm this hypothesis.

The metal content in solder pastes is another important factor affecting pore formation as emphasized by many authors [1, 3]. This is also true in the situation of Pastes 2 and 5 (see Fig. 4). Paste 2 has a higher metal content and a lower fraction of pores as compared with Paste 6. Pore density in Paste 6, however, is much less than those in Pastes 1 and 4 even though the metal content in Paste 6 is the lowest, especially when reflowed under IR 01.

3.3. Effect of infrared reflow time on pore formation

When using temperature profile IR 01, one round reflow takes about 600 s. Fig. 6 shows porosity change in two types of solder paste during infrared reflow. X-ray photographs for some typical changes of porosity are illustrated in Fig. 7. On the basis of these two figures, we notice that pore density in the solder joints varies with the reflow time. Pores can be found at a reflow time of 432 s when temperature rises to 183 °C, and melting of solder alloy begins. Afterwards, pore density decreases with increasing reflow time up to about 492 s. There is a peak around 516 s for both

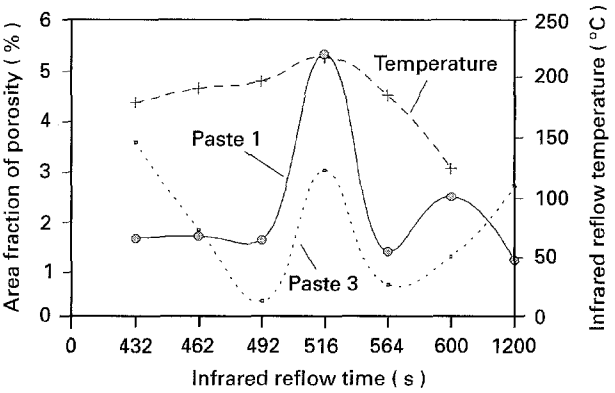

Figure 6 Variation of area fraction of porosity in a solder joint versus reflow time. Infrared reflow file. IR 01.

pastes, when the peak temperature is reached. The peaks and valleys which appear in Fig. 6 are caused by the opposite effects of melting of solder alloy and thermal decomposition of flux media. Melting of the alloy can decrease pore density, while decomposition of the flux will produce gases that may increase pore formation.

3.4. Thermal analyses of solder pastes

3.4.1. Thermogravimetric analysis (TGA) of solder pastes

Because pore formation in a solder joint is related to the gaseous materials in the pastes, the volume, speed and temperature of out-gassing or evaporation of solder pastes are important to pore formation. Thermogravimetric analysis (TGA) can describe the evaporation as the weight loss versus temperature. From Fig. 8, it can be seen that weight loss speeds of Pastes 6 and 3 are much greater when the temperature is below 180 °C and subsequently become smaller as compared with Paste 1. Because no melting and solidification of Sn63/Pb37 solder alloy occurs if the temperature is below 180 °C, the evaporation of flux and vehicle in solder pastes will not cause any porosity in the joints. When temperature rises further, on the other hand, the gases evaporated will cause pore

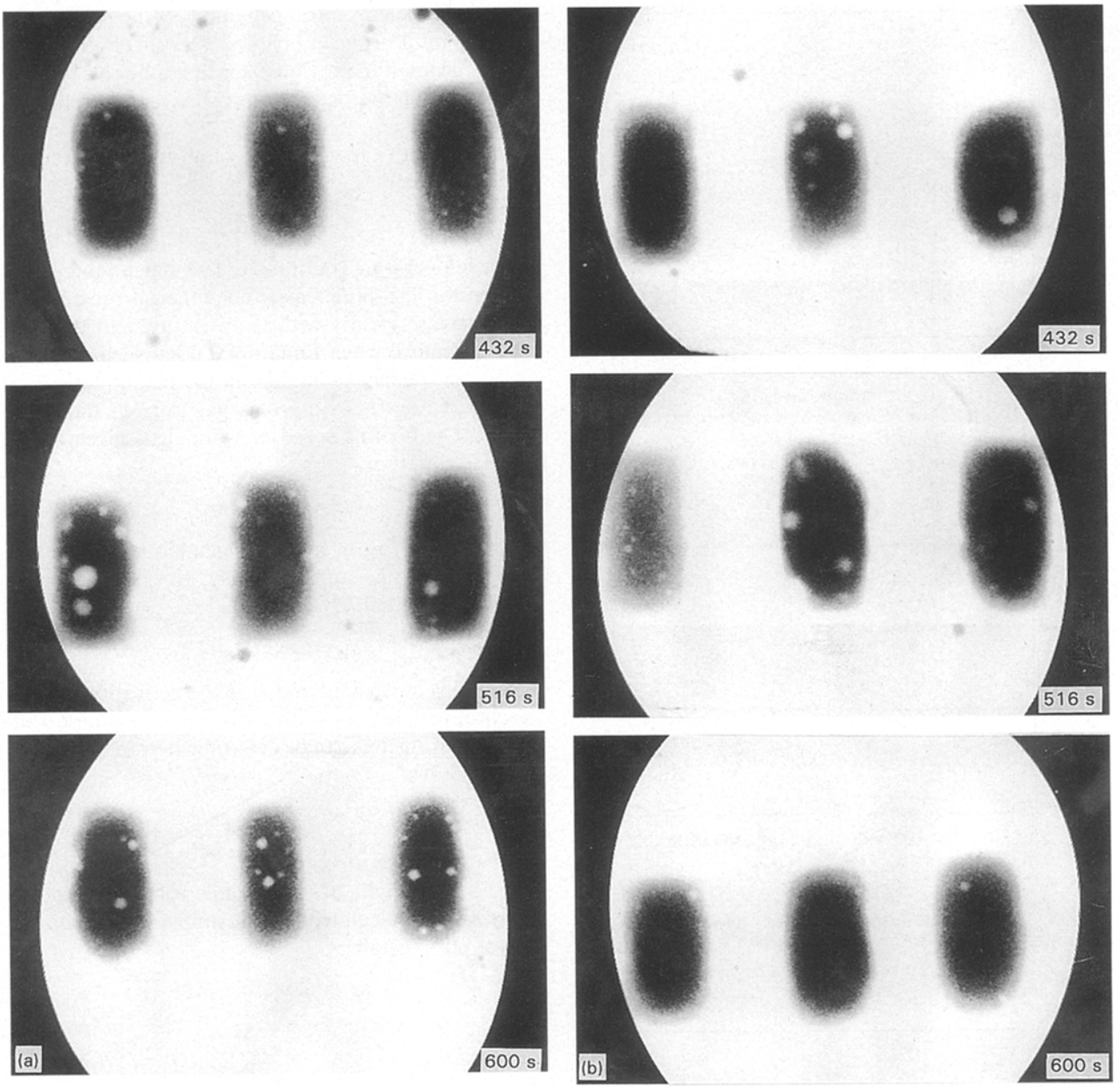

Figure 7 Pore formation in solder joints at different infrared reflow times (IR 01). copper land area 1.25×2.5 mm^2. (a) Paste 1, (b) Paste 3.

formation. This is because the solder alloy will solidify soon after the peak temperature. Therefore, Paste 6 has fewer pores than Paste 1, even though its metal content is lower.

3.4.2. Weight loss of solder pastes during infrared reflow

In actual infrared reflowing, the weight loss may be different as the heating method has changed. From Fig. 9, again, we can observe that the weight loss in Paste 6 is greater than that in Pastes 1 and 5 when the temperature is below 180 °C. As a result, the high content of flux medium in Paste 6 does not lead to a high pore density formation in its joints.

3.4.3. Differential scanning calorimetric (DSC) analysis of solder pastes

Summing up the observations of Figs 6–9, we can conclude that the flux and vehicle in Pastes 3 and 6 evaporate faster at low temperature (below 220 °C) and slower at high temperature (220–240 °C) than that in Paste 1. The differences between the solder pastes depend on their composition and structure, and may be observed from DSC curves.

Fig. 10 shows the results of DSC analysis for solder pastes: the highest endothermic peaks represent melting points of eutectic alloy Sn63/Pb37 for different pastes. We notice that melting occurs earlier for Paste 3 than for Paste 1, even though their alloy compositions are the same. The reason is that the particle size of metal powder in Paste 3 is smaller than that in Paste 1. It is worth noting that some small endothermic peaks appear below 180 °C in the DSC curve for Paste 3 and no peak appears above 220 °C. For Paste 1, however, the result is just the opposite. Small endothermic peaks can be seen only above 220 °C. This may explain why the evaporation rate of Paste 1 is smaller than those of Pastes 3 and 6 below 180 °C but becomes greater above 220 °C.

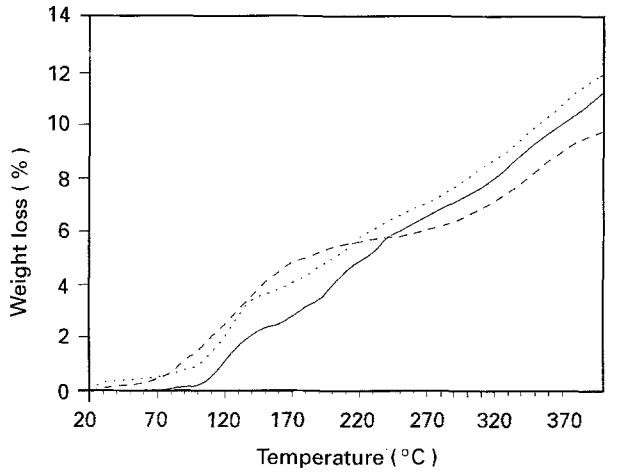

Figure 8 Thermogravimetric analysis of solder pastes, heating rate 5 °C min^{-1}. (—) Paste 1, (- - -) Paste 3, (···) Paste 6.

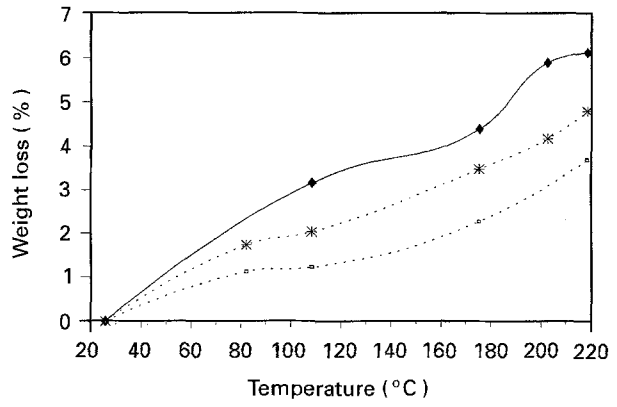

Figure 9 Comparison of weight loss between different solder pastes during infrared reflow (IR 01). (□) Paste 5, (*) Paste 1, (◆) Paste 6.

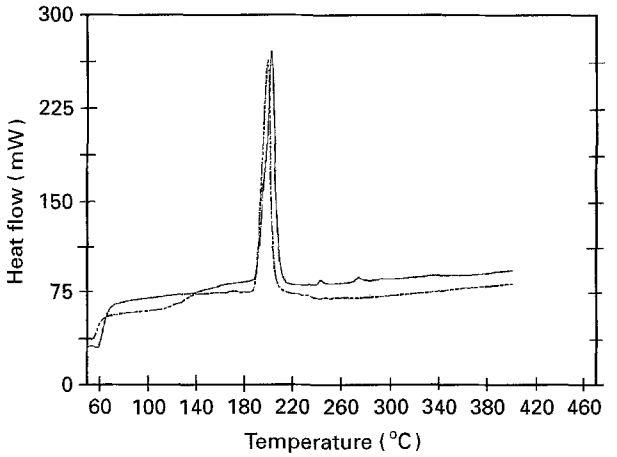

Figure 10 Differential scanning analysis on two different solder pastes. (—) Paste 1, (- - - -) Paste 3.

3.5. Mechanism of pore formation

If evaporated before the solder alloy begins to melt, gases can escape from the solder joints directly through the pores. The solder pastes have a volume fraction of pores of about 44% at that time. When the temperature reaches 183 °C or above, however, the outside surfaces of the joint begin to melt and are merged into a non-porous and smooth surface. The gases will then be entrapped and become gas bubbles in the joint. For the bubbles to escape from the solder joint, the internal pressure in each gas bubble must be greater than the external pressure, as described by Equation 2.

According to the equation of an ideal gas, the gas pressure becomes

$$P_g = nRT/V \tag{9}$$

If the temperature continues to rise, the number of gas molecules, n, also increases. Then the gas pressure, P_g, will increase greatly with temperature, and the bubbles can move when Equation 2 is satisfied.

The movement of bubbles in the blank pad can be considered as the rising of a gas pore in the liquid metal. The floating speed of a bubble is given by the Stock's equation

$$v = \rho g d^2/(18\eta) \tag{10}$$

The viscosity, η, of a liquid metal is related to the temperature, T, approximately by the Arrhenius equation [10, 11]

$$\eta = C\exp(H/RT) \tag{11}$$

where C is a constant and H is the activation energy. According to Iida and Guthrie's work [11], these well-known parameters can be determined from the following equations

$$C = \frac{5.7 \times 10^{-5}(MT_m)^{1/2}}{V_m^{2/3}\exp(H/RT_m)} \quad \text{(Pa s)} \tag{12}$$

The atomic weight, M, and atomic volume, V_m, of the alloy can be calculated from a simple weighted average of pure metals

$$M = x_1 M_1 + x_2 M_2 \tag{13}$$

$$V_m = \frac{M}{\rho_m} \tag{14}$$

where x_1, x_2 are mole fractions of tin and lead in the solder alloy and M_1, M_2 are the atomic volumes of pure metals, correspondingly. Then for eutectic alloy Sn63/Pb37, $M = 140.89$ g, $\rho = \rho_m \approx 8.07$ g cm^{-3} [12], $V_m = 16.58$ cm^3 and $T_m = 456.16$ K. By substituting these parameters into Equations 12 and 13 we can get $H = 1878.1$ and $C = 1.36 \times 10^{-3}$. Therefore, Equations 10 and 11 become

$$v = 3.36 \times 10^6 d^2 \exp\left(-\frac{225.89}{T}\right) (\text{m s}^{-1}) \tag{15}$$

$$\eta = 1.355 \times 10^{-3} \exp\left(\frac{225.89}{T}\right) \quad \text{(Pa s)} \tag{16}$$

The calculation of viscosity of eutectic alloy Sn63/Pb37 is in relatively satisfactory agreement with the experiment data ([3] pp. 164–5). Then, Equation 16 is available to estimate the rising speed of bubbles and is graphically shown in Fig. 11. It is seen from Fig. 11 that the speed at which a bubble rises increases greatly with increasing diameter. This rising speed for the bubble with a diameter of 0.2 mm is 82.7 mm s^{-1} at 183 °C. Then, the travelling time for such a bubble to escape from the joints is about 0.0024 s. Therefore,

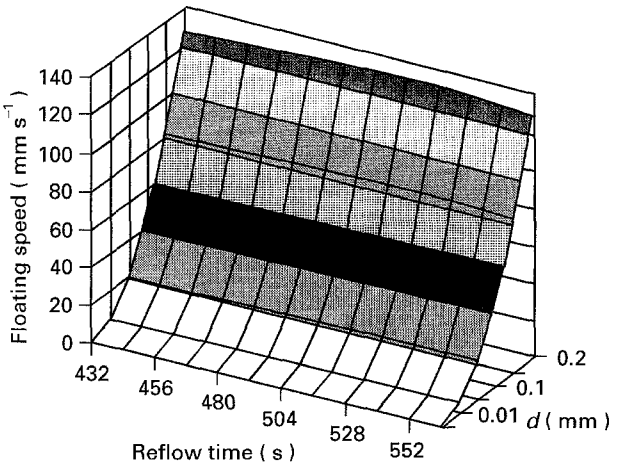

Figure 11 Rising speed of entrapped bubbles.

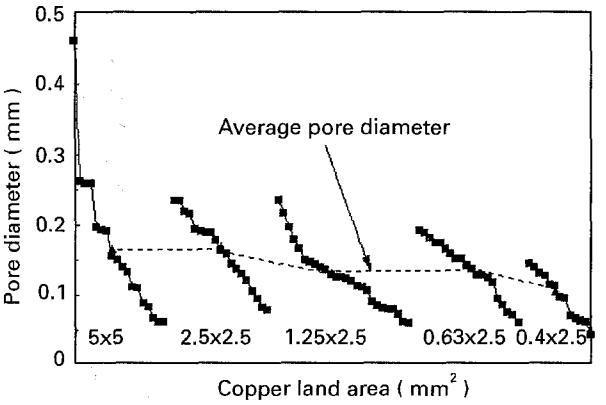

Figure 12 Pore-size distribution with different copper land sizes. Solder Paste 1, reflow file IR 01.

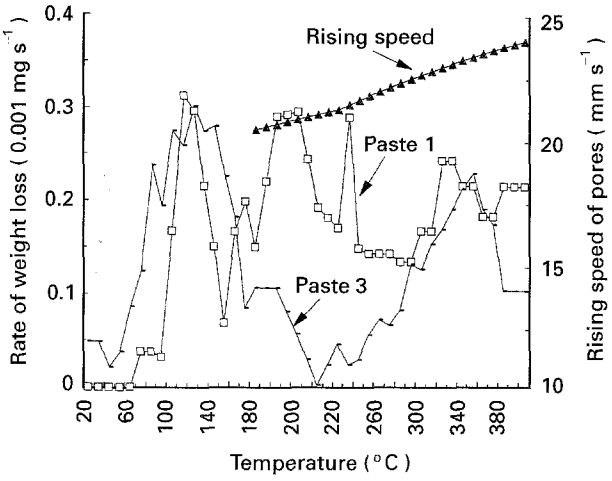

Figure 13 Variation of weight loss rate with temperature for different solder pastes.

it is easy for large bubbles to escape from the joints and usually only small bubbles remain in the blank joints. A high reflow temperature will also help the out-gassing of entrapped gases; however, as is shown in Fig. 11, temperature has only a slight effect on the rising speed in the infrared reflow soldering.

Fig. 12 shows the real dimension distribution of porosity in blank solder joints with different copper land areas. Pore sizes decrease with decreasing copper land size, and the average diameter decreases gradually from 0.17 mm for a $5 \times 5\,mm^2$ copper land to 0.15 mm for a $0.4 \times 2.5\,mm^2$ copper land. Although the rising speed of a bubble with a diameter of 0.15 mm is very high (46.47 mm s^{-1}), it can be entrapped in the joints. This is because the evaporation of flux and vehicle is also fast due to high temperature.

From the TGA curves (Fig. 8) for solder pastes, we can calculate the weight loss rate from the following equation

$$\frac{dw}{dt} = \frac{dw}{dT}\frac{dT}{dt} = \beta\rho V_0 \frac{dT}{dt} \qquad (18)$$

where β is the slope of TGA curve, $\beta \approx \Delta w/\Delta T = (w_{i+1} - w_i)/(T_{i-1} - T_i)$, the heating speed $dT/dt = 5/60\,^{\circ}C\,s^{-1}$ and the volume for each pad is $V_0 = 0.781\,mm^3$. Then, Equation 18 becomes

$$\frac{dw}{dt} \approx 5.4\frac{\Delta w}{\Delta T} \quad (10^{-3}\,mg\,s^{-1}) \qquad (19)$$

As shown in Fig. 13, the weight loss rate in paste 1, dw/dt, increases greatly with increasing reflow temperature from 180–210 °C, and reaches a peak at the peak reflow temperature. Therefore, many new gas bubbles are formed at the peak temperature. These bubbles are more readily entrapped in solder joints because the joints begin to cool from that time. In other words, flux and vehicle evaporated far below the peak temperature normally have little effect on pore formation. Pore formation usually occurs at or past the peak temperature when the joints begin to cool, especially if the evaporation rate is high at that time. Unlike Paste 1, Pastes 3 and 6 have a fast weight loss rate below the peak temperature and a slow weight loss rate around the peak temperature. Then their joints will have few pores.

It is difficult to eliminate the porosity in solder joints as the gaseous sources in solder joints cannot be eliminated completely during infrared reflow soldering. In fact, as can be seen from Fig. 6, the area percentage of porosity in Paste 3 increases if the sample is reflowed twice. Therefore, pore formation in solder joints is dependent mainly on the thermal characteristics of a solder paste. If one solder paste is selected, a suitable reflow process should be chosen to ensure higher evaporation and elimination of gases from the joints before the peak temperature is reached.

4. Conclusion

Based on a study of the effects of solder paste and infrared reflow temperature profile on pore formation and the investigation of formation and growth of pores in solder joints, the following conclusions can be drawn.

1. Pores in SMT joints are formed by entrapped gases that originate from the flux and vehicle in the solder paste during infrared reflow soldering. For a certain infrared reflow temperature profile, we observe that the peak area fractions of pores correspond to the peak temperature.

2. The characteristics of weight loss for a solder paste during heating are important in pore formation. TGA analysis is useful to evaluate the trend of pore formation in solder joints. It was found that, at the peak reflow temperature, the greater the weight loss, the greater was the area fraction of pores formed.

3. Among the solder pastes chosen, the area fraction of pores in Paste 6 is fewer than that in Paste 1 even though the metal content in Paste 6 is lower. Further, Pastes 2 and 3 have the lowest area fraction of pores in their solder joints.

4. The relationship between the floating speed of an entrapped bubble and its diameter is described in the equation $v = 3.36x10^6 d^2 \exp(-225.89/T)$ $(\mathrm{mm\,s^{-1}})$. The evaporation rate or weight loss rate may be estimated from the equation $dw/dt \approx 5.4\Delta w/\Delta T$ $(10^{-3}\,\mathrm{mg\,s^{-1}})$.

Acknowledgements

The authors thank the City University of Hong Kong (Research Grant 700144) for financial support. The use of X-ray radiographic facilities at the SMT laboratory of Hong Kong Productivity Council is gratefully acknowledged. One of the authors (D.J. X.), thanks Ms S.C. Lee, in the laboratory of the Department of Manufacturing Engineering (CPHK), for her helpful assistance.

References

1. JENNIE S. HWANG, "Solder Paste in Electronics Packaging" (Van Nostrand Reinhold, New York, 1989) p. 283.
2. RICHARD H. ESTES, *Solid State Technol.* **2** August (1984) 191.
3. HOWARD H. MANKO, "Soldering Handbook for Printed Circuits and Surface Mounting" (Van Nostrand Reinhold Company, New York, 1986) p. 185.
4. J. CAMPBELL, "Solidification of Metals" (Iron and Steel Institute, London, 1968) p. 218.
5. J. CAMPBELL, *Br. Foundryman* **62** (1969) 147.
6. W. D. BASCOM and J. L. BITNER, *Solid State Technol.* **18** September (1975) 37.
7. TIMOTHY L. HODSON, *Electron. Packaging Production* **39** September (1992) 77.
8. M. FORSHAW, *Circuit World* **15**(3) (1989) 14.
9. MICHAEL B. BEVER, "Encyclopedia of Materials Science and Engineering", Vol. 5 (Pergamon Press, Oxford, 1986) pp. 3830–9.
10. J. F. LANCASTER, "The Physics of Welding", 2nd Edn (Pergamon Press, New York, 1986) p. 40.
11. T. IIDA and RODERICK I. L. GUTHRIE, "The Physical Properties of Liquid Metals", (Oxford Science Publications, 1988).

Received 15 April 1994
and accepted 17 May 1995